The Second TSME International Conference on Mechanical Engineering
19-20 October, 2011, Krabi, Thailand

Comparison on Effect of Electrode Arrangements between Wire-to-Wire and Wire-to-Plate Types on Swirling Flow under Electric Fields in a Channel Flow

Suwimon Saneewong Na Ayuttaya*, Chainarong Chaktranond
Thatchapong Kreewatcharin and Phadungsak Rattanadecho
Department of Mechanical Engineering, Faculty of Engineering, Thammasat University
Khlong Luang, Pathum Thani 12121
Tel: 0-2564-3001-9 Fax: 0-2564-3010
E-mail: joysuwimon1@hotmail.com*

Abstract

This study aims to explore and compare the characteristics of swirling flow induced by electric fields performed from two electrode arrangements, i.e. wire-to-wire (WW) and wire-to-plate (WP) electrodes, in a channel flow. In both cases, location of an electrode wire, which is suspended from the upper wall of the channel, is initially located at the center line of the channel, and ground electrodes are fixed on the bottom wall. In wire-to-wire case, position of electrode is varied in the normal flow direction, while in wire-to-plate case, it is varied both in the normal and flow directions. Electrical high voltage is applied at 20 kV, and air flow velocity is tested in the range of 0.3 – 1 m/s. The numerical results show that electric field patterns from both cases are quite different. These results cause characteristics of swirling flows to appear differently. In WP case, when electrode is laid in line with plate ends, a swirling appears. While electrode is laid between two plate ends, two vortices are observed. Details of strength and shape of vortex in various cases are discussed in this paper.

Keywords: Swirling flow, Electric fields, Electrode arrangement.

1. Introduction

With demand of minimizing energy consumption, agricultural countries have developed efficient strategies to improve produces. Due to simple operation and construction, hot-air flow drying method is widely used for removing the moisture content from products. However, its drying period is long, resulting in large energy consumption [1].

In order to improve drying rate, many researchers have paid much attention in development of hot-air drying cooperating with other methods. For the past decade, some researchers studied seriously in Electrohydrodynamic drying process [2-5].

To improve the drying efficiency, an alternative method utilizes a combination of hot-air and electric field drying process. The effects

of parameters, such as applied voltage, air-flow velocity, temperature, and electrode arrangement on the drying efficiency of this method have been studied. Currently, two types of electrode arrangement have been studied, i.e. Wire-to-Wire type; WW [5 and 8] and Wire-to-Plate type; WP [6-7]. Lai and Lai [6] studied the effect of electric field parameters on the drying rate in packed-bed with WP configuration. The wire and copper plate was installed at the top and bottom of packed-bed, respectively. The results showed that drying rate could be greatly enhanced when high voltage applied. However, a cross-flow with a high velocity was diminished the effect of Corona wind.

Ahmedou et al. [7] investigated the EHD enhancement on the drying process by WP. The results showed that when cross air velocity was low and the distance between product and Corona wind was small, the ionic wind leaded to an enhancement of the drying rate.

Chaktranond and Rattanadecho [5] experimentally investigated the influences of electrical voltage on the heat and mass transfer in porous packed bed subjected to electrohydrodynamic drying. With WW configuration, four wire electrodes and a wire ground were installed at the normal flow direction and cross flow direction, respectively. Electric fields were applied in the range of 0–15 kV. Average velocity and temperature of hot airflow were controlled at 0.33 m/s and 60 ^{o}C, respectively. The results showed that the heat and mass transfer rate in the pack-bed was increased. The convective heat transfer coefficient and drying rate were considerably enhanced with the strength of electric field due to the effect of Corona wind.

Saneewong Na Ayuttaya et al. [8] numerically studied the influences of positions of WW arrangement on the Corona wind pattern. The results showed that adjusting the distance between electrode and ground in horizontal direction affected the size and strength of vortex. When the distance was closer, the induced vortex strength increases with Corona wind due to stronger and denser electric fields. Moreover, with increasing the number of electrode, electric fields were increased and vortices are assembled. This caused Corona wind become larger and more violent.

From above literatures, there are no researches study and compare electric field distribution from electrode arrangements. In this research, swirling flow under electric field and electrode arrangements are studied. In addition, parameters affecting electrode arrangements and the suitable flow velocity are also investigated.

2. Principle of Electrohydrodynamic

Mechanism of Electrohydrodynamic method is shown in Fig.1. When high electrical voltage is exposed to airflow (Fig.1 (a)), the gas motion is created by ions generated in the Corona discharge near the sharp electrode that drift to the ground. As a result, the momentum of gas is enhanced and cross flow or primary flow is generated. Shear flow is then appeared due to difference of fluid velocity between charged air flow and free air flow. Electric body force, moreover, influences the direction of flow pattern. This causes shear flow to become the circulating

flow as shown in Fig.1 (b). [Chaktranond and Rattanadecho, 2010]

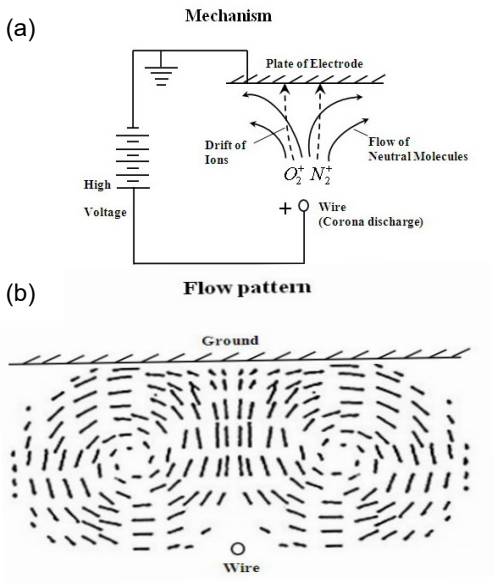

Fig.1 Electrohydrodynamic method [8].
(a) Mechanism of high electrical voltage
(b) Corona wind pattern

3. Computational model

Our computational domain is showed in Fig.2. The effect of electrode arrangement by Electrohydrodynamic is studied for two different domains.

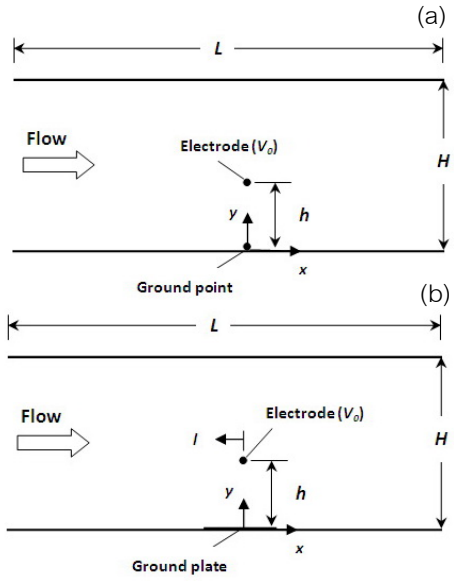

Fig.2 Computational model (a) WW (b) WP.

3.1 Channel flow domain

The first domain reproduces 2-D channel flow. Dimensions of duct are 0.15 m (*H*) and 2.00 m (*L*). The upper and lower surfaces of channel flow domain are insulated. Airflow is assumed to be incompressible flow. In addition, motion of fluid flow is computed through continuity (Eq.1) and Navier-Stokes equation (Eq.2),

$$\nabla \cdot \vec{u} = 0\,, \tag{1}$$

$$\rho\left[\frac{\partial \vec{u}}{\partial t} + (\vec{u}\cdot\nabla)\vec{u}\right] = -\nabla\vec{P} + \mu\nabla^2\vec{u} + \vec{F}_E\,, \tag{2}$$

where $\vec{u}$ is velocity vector of fluid, t is time, $\vec{P}$ is pressure, ρ is density, and μ is viscosity of air. $\vec{F}_E$ is the Electrophoretic force or Coulomb force. The boundary conditions are shown in Table 1.

Table 1. Boundary conditions.

	$u(m/s)$	$V(kV)$	$q(\mu C/m^3)$
Electrode	$u_0 = 0$	$V = V_0$	q_0
Ground	$u = 0$	$V = 0$	$q = 0$
Inlet	$u = u_{in}$	$\partial V/\partial x = 0$	$\partial q/\partial x = 0$
Outlet	$\partial u/\partial x = 0$	$\partial V/\partial x = 0$	$\partial q/\partial x = 0$
Upper wall	$u = 0$	$\partial V/\partial y = 0$	$\partial q/\partial y = 0$
Lower wall	$u = 0$	$\partial V/\partial y = 0$	$\partial q/\partial y = 0$

3.2 Electric field domain

The second domain reproduces 2-D electric field domain. Dimensions of domain are 1.6 m (high) and 2.00 m (*L*) for two types of electrode arrangement, i.e. WW (Fig.2 (a) and WP (Fig.2 (b). Electrode wire cross-sectional is assumed to be a circle (diameter = 0.5 mm). At the tip of electrode has space charge density q_0 [9]. Ground is always fixed at *y* = 0 while the

distance in flow direction, *x,* and normal direction, *y* are varied, i.e. *l* and *h* respectively. Coulomb force is calculated by

$$\vec{F}_E = q\vec{E}\,, \tag{3}$$

where *q* is electric charge density and electric field intensity ($\vec{E}$) is calculated by Maxwell's equation (Eqs.4 and 5),

$$\nabla \cdot \varepsilon\vec{E} = q\,, \tag{4}$$

$$\vec{E} = -\nabla\vec{V}\,, \tag{5}.$$

Where ε is dielectric permittivity and $\vec{V}$ is electric potential. The boundary conditions are shown in Table 1. The equations are solved by using COMSOL. Lagrange quadratic element is chosen as the basis functions with triangular shapes as shown in Fig. 3. About 8,000 elements are used on free mesh parameter with a maximum error of 0.01%.

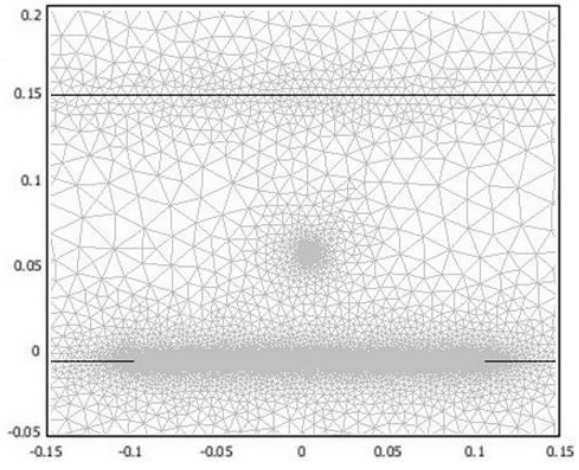

Fig.3 Grid system.

In simulations, the steady state flow is solved by using the standard electrostatic model. In all cases, Laminar flow enters the inlet of duct with a uniform velocity, where ρ is 1.205 kg/m^3 and μ is 1.8 $\times 10^{-5}$ kg/m s. Zero pressure is identified at the outlet air boundary.

4. Comparison of electrode arrangement

In order to study the effect of electrode arrangement, initial condition must be given as *l* = 0 cm, *V* = 20 kV and *u* = 0.5 m/s [7].

4.1 Electric field distribution

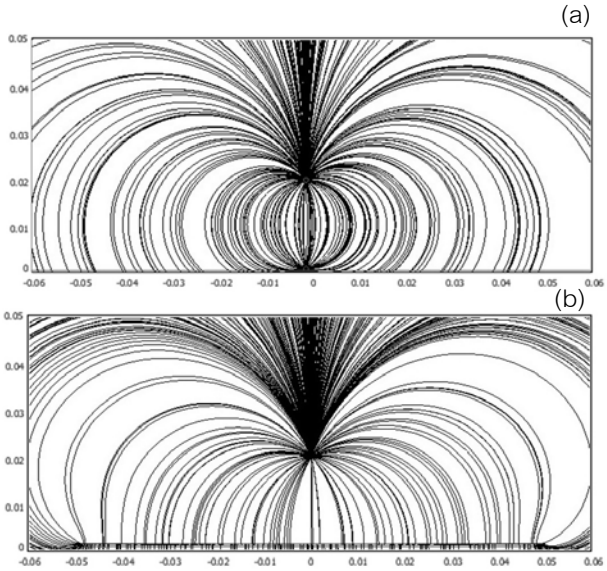

Fig.4 Electric field at *h* = 2 cm; (a) WW (b) WP.

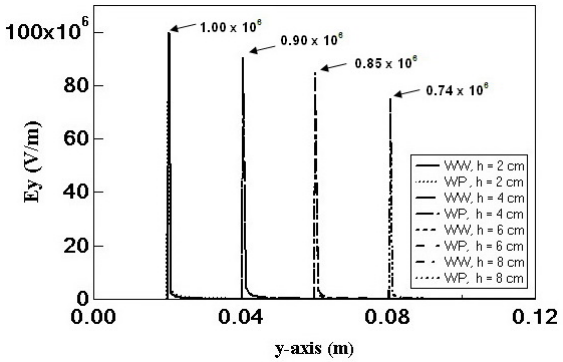

Fig.5 Electric fields in various *h* and electrode arrangement when consider *y* at the electrode.

Figure 4 shows the comparison of electric fields distribution from WW and WP arrangement. It can be seen that the electric fields are from

electrode to ground. As shown in Fig.4 (a), with WW arrangement, electric field lines are crowded at both electrode and ground. With WP arrangement, electric field lines are crowded at electrode but they spread over the ground surface, as shown in Fig.4 (b).

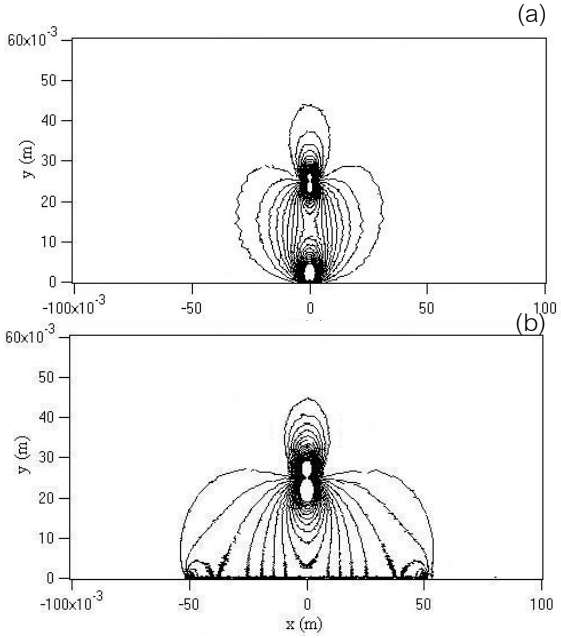

Fig.6 Electric force at *h* = 2 cm; (a) WW (b) WP.

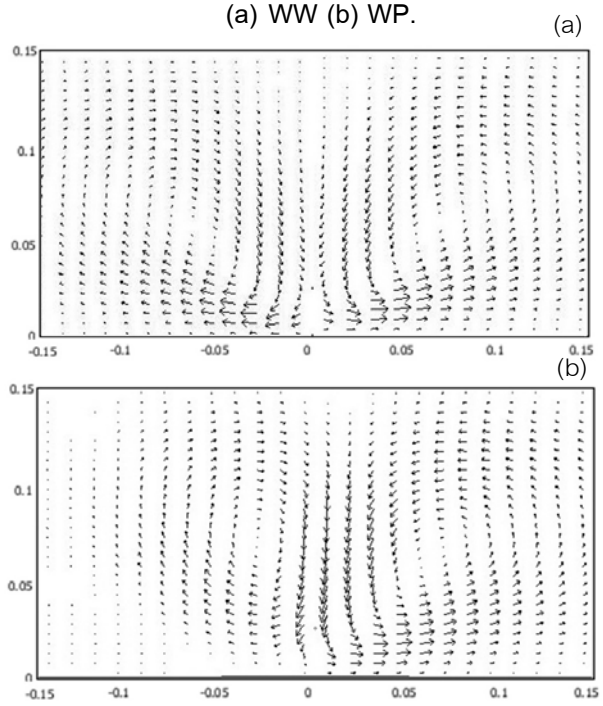

Fig.7 Velocity vector under electric field when *u* = 0 m/s at *h* = 2 cm; (a) WW (b) WP.

Figure 5 shows electric field intensity at the electrode. When the gap (*h*) is closer, electric field intensity increases significantly because electric charge density is overcrowded. In other words, electric fields intensity and the gap are said to be an inverse proportion, $E \propto 1/h$. Regarding to the maximum electric fields intensity, Both arrangements showed no difference for each *h*. When we consider electric force, it can be seen from Fig.6 that electric forces are from electrode to the ground for both arrangements. According to Fig.6 (a), electric forces are from electrode to the ground point for WW while they are spread over the ground plate area for WP as shown in Fig.6 (b). So ground from WP arrangement causes to spread the electric force.

Figure 7 shows the velocity vector of air under electric fields when there is no inlet flows. Swirling flow between electrode and ground is induced by shear flow occurred from the difference between charged and uncharged air velocities. In addition, with different electric force distribution, the circulating flow for WP arrangement is widely swirled and extended more than that of WW arrangement.

4.2 Swirling flow when consider the air flow

A comparison of swirling flow of WW when *h* = 2 and 6 cm is shown in Fig.8. It can be seen that only a swirling flow can be identified and appears at the downstream. When Coulomb force of WP splits more than WW, The cause of electric field is endured, so there are two swirls, as shown in Fig.9. The size of the upstream one is smaller than that of the downstream. The

upstream swirl encounters an erosion from air flow while it, on the other hand, encourages the downstream swirl. When consider swirling flow in various *h*, swirling flow of *h* = 2 cm circulates in the narrow zone while it widely circulates when *h* = 6 cm.

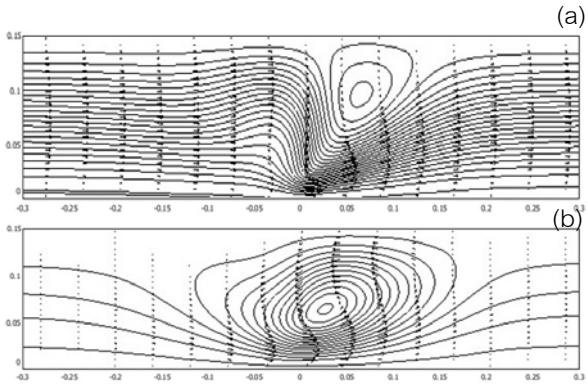

Fig.8 Swirling flow of WW at *u* = 0.5 m/s; (a) *h* = 2 cm and (b) *h* = 6 cm.

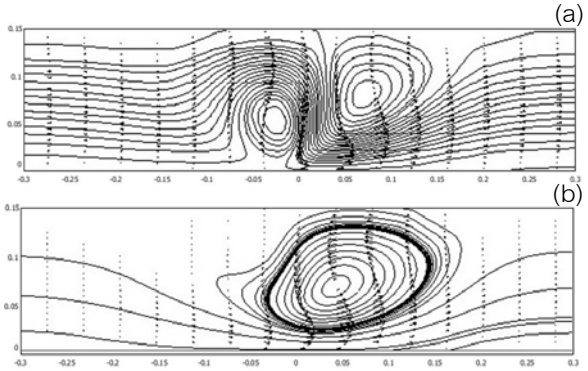

Fig.9 Swirling flow of WP at *u* = 0.5 m/s; (a) *h* = 2 cm and (b) *h* = 6 cm.

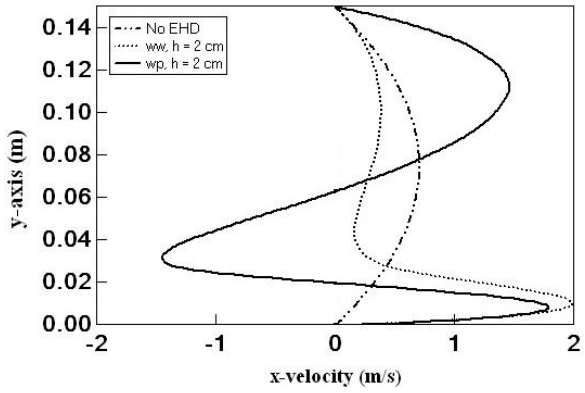

Fig.10 *x*-velocity profile when consider *y*-axis at *x* = 0 m.

Figure 10 shows velocity profile of air flow along *y*-axis at *x* = 0 m. Parabolic pattern is appeared when there is No EHD. When high voltage is applied, electric field changes the pattern of the flow. Fluid moves from left to right and the maximum values are limited to the lower part of the channel close to where the ground is located instead of at the center. In addition, the influences of swirling flow cause the air to flow in two different directions, clockwise flow and counterclockwise flow direction. Under the swirling flow, high velocity of air flow can be noticed due to smaller effective area. With respect to the arrangement, velocity of WW arrangement is higher than WP arrangement. WW arrangement tends to provide more flow supports than the WP arrangement. Considering *x*-velocity along *y*-axis, it can be seen that average velocity of WW is greater than that of WP about 3.43%. However, WP changes the flow pattern more than WW which, change only near ground.

4.3 Effect of velocity (*u*)

When we increase inlet velocity of the air flow, the pattern of swirling flow is changed. According to Fig.11 and Fig.12, it can be seen that the strength of swirling flow is decreased when velocity of air is increased because inertial force is preponderant compared to the electric body force. This is clearly seen from WW which only a circulating flow occurred. In case of WP, the electric body force spreads over the ground area causing a wide circulating flow. Thus, when the inertial force is greater than the electric body force, the circulating induction is diminished.

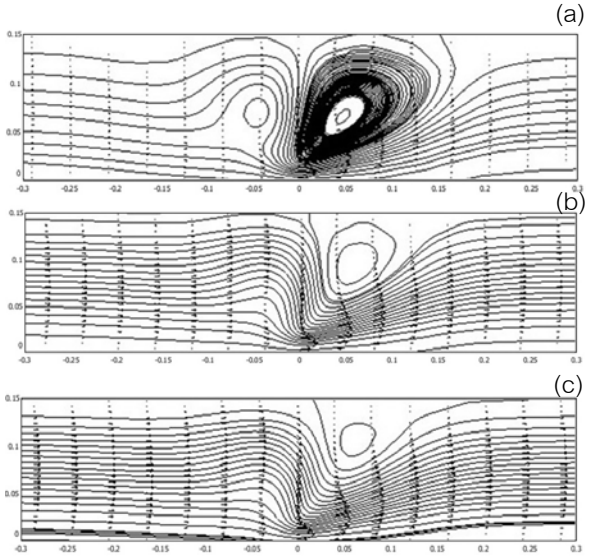

Fig.11 Swirling flow when *l* = 0 cm, *h* = 2 cm, *V* = 20 kV (a) *u* = 0.3 m/s (b) *u* = 0.8 m/s and (c) *u* = 1 m/s when consider WW.

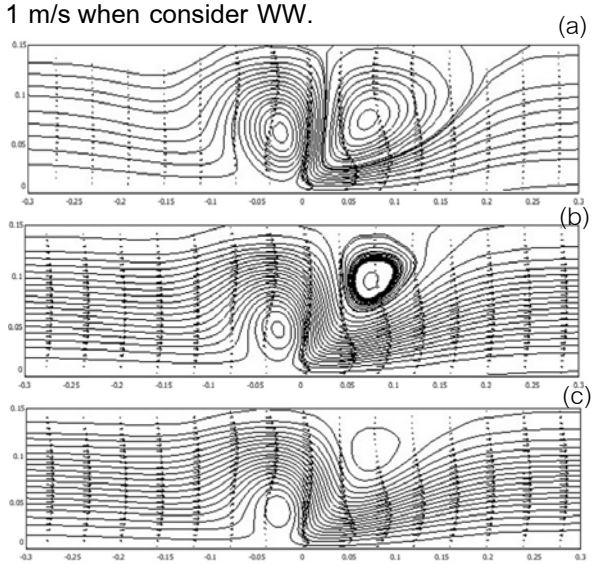

Fig.12 Swirling flow when *l* = 0 cm, *h* = 2 cm, *V* = 20 kV (a) *u* = 0.3 m/s (b) *u* = 0.8 m/s and (c) *u* = 1 m/s when consider WP.

4.4 Effect of electrode arrangement in WP cases

From previous present, the position of electrode is installed at the center of the ground (*y* = 0 m). Fig.13 shows the characteristic of the swirling flow when electrode is installed on the left edge (*l* = 5 cm) and the right edge (*l* = -5 cm) of ground. At *l* = 5 cm, the direction of swirling flow is counterclockwise whereas at *l* = -5 cm, swirling flow is circulated in the opposite direction because the electric force induces circulating flow in the different direction.

Fig.14 shows velocity profile of air flow when we consider *y*-axis at center of swirling flow**.** Considering near ground position, it is found that at *l* = 5 cm, the effect of electric force induces the flow such that the flow moves to the right direction. At *l* = -5 cm, the electric force induces the flow in the different direction and decreases the *x*-velocity of the flow.

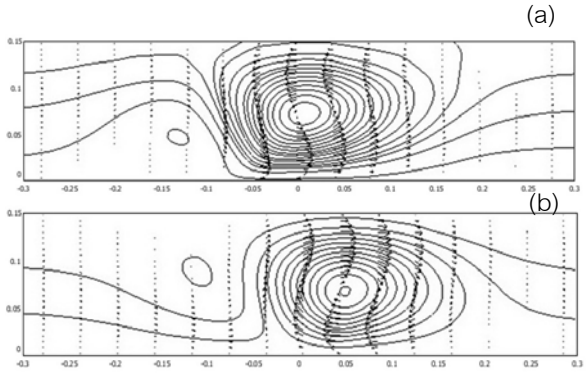

Fig.13 Swirling flow when *l* = 0 cm, *h* = 2 cm, *V* = 20 kV, *u* = 0.3 m/s (a) *l* = 5 cm and (b) *l* = -5 cm.

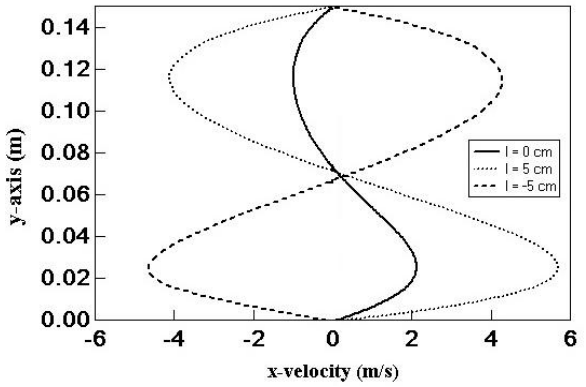

Fig.14 Velocity profile in *x*-velocity when consider *y*-axis at center of swirling flow**.**

5. Conclusions

Numerical simulation is carried out to study the influence of the electrode arrangement and the effect of inlet fluid velocity inside the channel flow on the characteristics of swirling flow. The conclusions are obtained as follow:

5.1 The effect of electrode arrangements (WW and WP) influences the electric field distribution. In both cases the maximum electric field intensity are not different for each gap value. When the gap (*h*) is closer, electric field (*E*) increases significantly, i.e. $E \propto 1/h$.

5.2 The difference of electrode arrangements influences the swirling flow behavior. When *h* = 2 cm, WW arrangement is appeared the only a swirling flow but two swirling flow is appeared at WP arrangement.

5.3 The strength of swirling flow is not dominated when velocity of air is increased. With respect to the arrangement, *x*-velocity of WW arrangement is higher than WP arrangement. WW arrangement tends to provide more flow supports than the WP arrangement. However, WP changes the flow pattern more than WW which, changes only near ground.

5.4 The pattern of swirling flow is changed, when we study electrode arrangement in WP cases, due to the electric force induces the flow in the different direction.

6. Acknowledgement

The authors would like to express their appreciation to the National Research University Project of Thailand Office of Higher Education Commission, the National Research council of Thailand, and Faculty of Engineering, Thammasat University for providing financial support for this study.

7. References

[1] Lai, F.C. and Sharma, R.K. (2005). EHD enhanced drying with multiple needle electrodes, *J. Electrostatics,* vol. 63, pp.223-237.

[2] Lai, F.C. (2010). A prototype of EHD-enhanced drying system, *J.Electrostatics*, vol. 68, pp.101-104.

[3] Chaktranond, C. and Ratanadecho, P. (2009). Heat and mass transfer enhancement in unsaturated porous packed beds subjected to Electrohydrodynamics (EHD), *The 6th Asia-Pacific Drying Conference (ADC2009),* 19-21 October, 2009, Bangkok, Thailand.

[4] Ahmedou, A.O. and Havet, M. (2009). Analysis of the EHD enhancement of heat transfer in a flat duct, *IEEE Transactions on Dielectrics and Electrical Insulation*, vol.16, pp.240-247.

[5] Chaktranond, C. and Ratanadecho, P. (2010). Analysis of heat and mass transfer enhancement in porous material subjected to electric fields (effects of particle sizes and layered arrangement*), Experimental Thermal and Fluid Science,* vol. 34, pp. 1049–1056.

[6] Lai, F.C. and Lai, K.W, (2002). EHD-enhanced drying with wire electrode, *Drying Technol,* vol.20 (7), pp. 1393–1405.

[7] Ahmedou, A.O. and Havet, M. (2009). Assessment of the electrohydrodynamic drying process, *Food Bioprocess Technol,* vol. 2, pp. 240-247.

[8] Saneewong Na Ayuttaya, S., Chaktranond, C. and Rattanadecho, P. (2010). Influence of electrode wire structure on Corona wind in a 2-D rectangular duct flow (Numerical Analysis*). The 1st International Conference on Mechanical Engineering*, 20-22 October, 2010, Ubon Ratchathani, Thailand.

[9] David, J.G, Introduction to Electrohydrodynamics., 3 ed., Prentice Hall International, Inc., New Jersey, 105 p., 1999.